

Effectiveness of Ceria and Stania Nanoparticles in Photodegradation Tenoxicam Antibiotics Using UV-H₂O₂

Hussein Abdel-Fattah Khalaf^{*a}; Randa Fouad Abd El-Baki^b

a) Chemistry department, Faculty of Science, Damanshour University, Damanshour, Egypt

b) Chemistry department, Faculty of Science, New Valley University, El-Kharja, 72511, Egypt

Received 5 May 2023; received in revised form 20 August 2023; accepted 2 September 2023 (DOI: 10.30495/IJC.2023.1985433.2006)

ABSTRACT

Both metal oxides, ceria (CeO₂) and stania (SnO₂) are prepared by precipitation technique using ammonia solution (1:1) and characterized by thermogravimetric analysis (TGA), x-ray powder diffraction (XRD), transmission electron microscope (TEM), nitrogen adsorption-desorption (for the specific surface area determination, S_{BET}) and used in the photodegradation of Tenoxicam (TEN) antibiotics by using ultraviolet irradiation in presence of hydrogen peroxide. The obtained results showed that ceria and stania have a comparable surface area of 12 and 11 m² g⁻¹, respectively, and the crystallite size measured by XRD was found to be 44 and 18 nm for ceria and stania, respectively. Also, the results show that by increasing the exposure time, the amount of degraded antibiotic was increased. Data obtained show that both oxides, ceria, and stania can be used effectively as catalysts in the photodegrading process as photocatalysts. Stania is faster than ceria to degrade TEN antibiotics. Ceria needs more time than stania to degrade the drug at 100%, in which the TEN is fully degraded in the presence of stania and H₂O₂ at 40 minutes under certain conditions.

Keywords: Photodegradation; Photocatalyst; Kinetics; Tenoxicam; Cerium oxide; Tin oxide.

1. Introduction

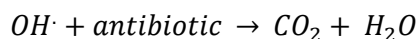
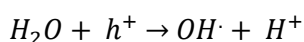
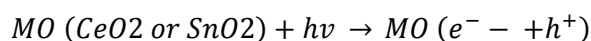
Contaminated wastewater, with textile residues, dyes, heavy metals, and medical wastes is one of the environmental problems. Due to the negative effects on humans and aquatic ecosystems, the contamination of the environment by Pharmaceutical because of metabolic excretion, improper disposal, and/or industrial waste has been the subject of special attention over recent years. From these pharmaceuticals wastes, antibiotics represent a danger for the ecosystem [1-4]. The presence of antibiotics in surface waters and groundwater is a significant problem caused by human pollution. Therefore, it is crucial to detect antibiotic residue in food production and biological fluids [5]. Many countries have started monitoring the levels of active pharmaceutical ingredients in water due to the detection of various drugs at different concentrations. Several methods have been used to overcome this

problem [6, 7]. For the removal of these pharmaceutical pollutants that cannot be treated by conventional procedures due to their high chemical stability and limited biodegradability, the advanced oxidation process (AOP) is one of these ways. The classification of AOPs can be divided as follows: ozonation [8, 9] Fenton and photo Fenton oxidation [10] photolysis and H₂O₂ enhanced photolysis [11] heterogeneous photocatalysis [12] sonolysis [8], etc. Photocatalysis-based AOP using different metal oxides/sulfides (TiO₂, ZnO, ZnS, SnO₂, CeO₂, Fe₂O₃, CdS, WO₃, graphene-based metal oxides, etc.) had become a promising method for the degradation of several organic pollutants [3, 13, 14]. They can totally degrade the contaminants that produce no secondary pollution when exposed to sunlight or ultraviolet radiation at room temperature [15]. Stania, SnO₂ is an important n-type semiconductor material with excellent chemical and physical performances. SnO₂ nanostructures can photodegrade organic pollutants to other nontoxic small molecules, as

*Corresponding author:

E-mail address: hkhaf70@sci.dmu.edu.eg (H. A. Khalaf)

an efficient photocatalyst, by UV irradiation. Nanomaterials' morphology and size have a big impact on their characteristics [16, 17]. Ceria (CeO_2) is one of the important metal oxides in catalysis, characterized by abundant in the earth's crust, thus giving itself as a strong economical challenger [18]. CeO_2 with two valence states Ce^{4+} and Ce^{3+} has better catalytic activity in the ultraviolet light region [19], therefore, much effort has been made to improve the photocatalytic activity of CeO_2 [20]. Ceria and stania photocatalysis has become an attractive process to stimulate the degradation of aquatic pollutants since it allows their rapid and efficient deduction from water, transforming them into byproducts with lower toxicity [21]. Both CeO_2 and SnO_2 have a band gap energy of 3.23 and 3.6 eV, respectively [22, 23]. Thus, stania can absorb a big part of the solar spectrum. Due to their enormous energy band gaps, CeO_2 and SnO_2 powders mostly absorb ultraviolet light to create electron-hole pairs in the wavelength range of 400 nm or below, with essentially little absorption in the visible light spectrum (400-700 nm) [24]. The photocatalytic process includes several reactions occurred as follows [4]:



The process of e/h recombination can damage the photocatalysis process. In order to address this issue, various methods have been employed such as utilizing semiconducting materials at the nano-scale, utilizing heterojunction semiconducting systems, introducing metal or non-metal doped semiconductors, and employing supported semiconductors [25]. The nano-sized approach reduces the distance that photoinduced e-/h+ pairs have to travel from the semiconductor's bulk to its surface. This allows the e-/h+ pairs to reach the surface faster, enabling their participation in the photodegradation process before recombination happens again [26].

One of the non-steroidal anti-inflammatory medications is tenoxicam (TEN) belonging to the chemical class of oxicams. TEN is almost odourless and a yellow crystalline powder, and chemically, tenoxicam is 4-hydroxy-2-methyl-N-2-pyridinyl-2H-thieno(2,3-e)-1,2-thiazine-3-carboxamide 1,1-dioxide. It has been used to treat inflammatory and rheumatic illnesses, including osteoarthritis, and is regarded as an effective anti-inflammatory medication [27]. From the literature review, there is a very few studies reported about the photodegradation of tenoxicam, Mahmoud et al [28]

studied the photodegradation of tenoxicam under UV only and they found that the photodegradation rate increases with increasing temperature and light intensity. de Melo Santos et al [29] using photo-assisted peroxidation and photo-fenton processes for the photodegradation of tenoxicam from an aqueous solution. de Melo Santos et al [30] used the system $\text{sun}/\text{H}_2\text{O}_2/\text{Fe-TiO}_2$ for the removal of three mixed antibiotics (ketoprofen, meloxicam, and tenoxicam).

The objective of this study is to investigate the photodegradation of TEN in aqueous solution using a photocatalytic process based on CeO_2 and SnO_2 , individually, with different systems. In addition, to study the effect of operating conditions like concentration, pH, H_2O_2 , and irradiation time on the degradation percent of selected antibiotics.

2. Experimental

2.1 Tenoxicam aqueous solution

A TEN standard (20 mg) was obtained from Egyptian Int. Pharmaceutical Industries Co. (EIPICO). A stock solution of TEN was prepared by dissolving the compound in deionized water to give 100 mg/L. All other materials are analytical grades and were purchased from Merck. TEN absorbs UV through two peaks at about 230 and 270 nm. These two peaks were attributed to the conjugation of double bonds in the chemical formula of the antibiotic and suggested that the antibiotic was not affected by a high UV lamp (365 nm) in agreement with the results obtained below. The calibration curve for TEN was constructed by different standard solutions of TEN containing 5.0 to 30.0 mg/L. The calibration curve was constructed by plotting mean absorbance (at λ_{max} 270 nm) versus TEN concentrations.

2.2 Synthesis of the ceria and stania catalysts

Tin oxide (SnO_2) and cerium oxide (CeO_2) are prepared by the method described in the literature [24, 31] by a slow dropwise addition of a 1:1 ammonium hydroxide solution to a warm (60-80 °C) 0.3 M aqueous solution of $\text{SnCl}_4 \cdot 5\text{H}_2\text{O}$ or $\text{Ce}(\text{NO}_3)_3 \cdot 6\text{H}_2\text{O}$ AR grade, BDH product (England), with a continuous stirring till pH = 8 is reached. The white precipitate was left overnight before being filtered, washed, dried, ground, and calcined at 600 °C for 3 h.

2.3 Catalyst characterization

Thermogravimetric analysis (TGA): V2-2A DUPONT 9900 thermal analyzer with $\alpha\text{-Al}_2\text{O}_3$ as reference was used to study the thermal events of ceria and stania and

the TGA curves, were performed between room temperature and 1000 °C in a static air. 5-15 mg of the sample were used in TG measurements with a 10°C/min rate of heating.

X-ray diffraction (XRD): the phase identification was characterized using a JSX-60PA/Jeol diffractometer (Japan) equipped with a Ni-filtered CuK α radiation ($\lambda=1.5418 \text{ \AA}$). The generator was operated at 35 kV and 20 mA, and the diffractometer at 2 θ diverging and receiving slits and a scan rate of 2 ° θ / min. The average crystallite size of metal oxides was calculated by application of the Debye-Scherrer's equation (Eq. 1) [32-34].

$$D = \frac{K \lambda}{\beta \cos \theta} \quad (1)$$

Where D is the average crystallite size, $\lambda=1.54056 \text{ \AA}$ is the wavelength of CuK α radiation, β is the full width at half-maximum (FWHM) intensity of the peak in radian, θ is Bragg's diffraction angle and K is a constant usually equal to 0.9.

Transmission electron microscopy (TEM): a JEM 100 CXII transmission electron microscope (TEM) operating at 80 kV used for the characterization of nanoparticle size.

Nitrogen sorption: NOVA 3000, version 6.10 high-speed gas sorption analyzer (Quantachrome Corporation, USA) were used to obtain complete nitrogen adsorption/desorption isotherms at -196 °C. Before the analysis, the calcined samples were outgassed at 200 °C for 1 hour. From the resulting twenty-four-point adsorption and desorption isotherms, we calculated the BET surface areas (S_{BET}) using established and widely accepted methods.

2.4 Photocatalytic experiments

The photocatalytic degradation of TEN was carried out in a 500 ml Pyrex glass reactor. The source of UV light was a UV lamp (Cole-Parmer 4-watt with 254 and 365 nm, 230 VAC/60 Hz), which was placed above the reactor. The catalyst (CeO $_2$ or SnO $_2$) was immersed in 100 mL aqueous solution of TEN (50 mg/L) containing 300 mg/L H $_2$ O $_2$, the pH was adjusted to the required value (pH 9) by adding NaOH or HCl (1N) and the solution was magnetically stirred in the dark for 30 min to establish the adsorption-desorption equilibrium. Then the solution was irradiated with UV light.

To monitor the degradation progress, 5 ml aliquots of the reaction mixture was withdrawn at time intervals. Samples were centrifuged for 2 min at 150 rpm and filtered using 0.45 microns. The extent of degradation of TEN was monitored spectrophotometrically using a Du 800 spectrophotometer, Beck-man Coulter, at λ_{max} (270 nm) of the TEN solutions. The degradation efficiency (%) has been calculated according to Eq. (2).

$$\% \text{Degradation} = \frac{C_0 - C_t}{C_0} * 100 \quad (2)$$

where C_0 is the initial concentration of TEN and C_t is the concentration of TEN after photo-irradiation. The adsorbed amount of antibiotics q_t (mg/g) was measured by the difference between the initial and final concentrations according to Eq. (3).

$$q_t = \frac{V(C_0 - C_t)}{m} \quad (3)$$

where C_0 and C_t are the initial and equilibrium antibiotic concentration (mg /L), V is the volume of solution (L) and m is the catalyst dose (g).

The photodegradation kinetics study of TEN was investigated for UV/H $_2$ O $_2$ /catalyst systems. The loss of antibiotic was observed as a function of irradiation time and data were fitted to a pseudo first-order rate model using Eq. (4) where k is a pseudo first-order rate constant (min $^{-1}$). The half-life time of the process was obtained for 1 $^{\text{st}}$ -order kinetics using Eq. (5).

$$\ln \frac{C_0}{C_t} = K_1 t \quad (4)$$

$$t_{1/2} = \frac{0.693}{K_1} \quad (5)$$

3. Results and Discussion

3.1 Catalysts characterization

The TGA curves of the stania (SnO $_2$) and ceria (CeO $_2$) gel are shown in **Fig. 1**. From the TGA profile of SnO $_2$ gel, there are two mass loss steps in the temperature range RT-1000°C. These two steps are attributed to the loss of volatile materials like physisorbed water and dehydroxylation processes. Theoretical mass loss (19.3%) is agreed with experimental mass loss (19.9%) hence this implies that the tin gel sample approaches the suggested formula (SnO $_2 \cdot 2\text{H}_2\text{O}$), which gives well agreement with the XRD data. For CeO $_2$, thermal analysis results (**Fig.1**) exhibited the loss of physisorbed water and partial surface dehydroxylation through two steps. The first step, 4.3% mass loss, appeared at 100°C due to the loss of physisorbed water,

and the other mass loss step (ca 72.4%) is the main decomposition process that occurred in a narrow temperature region (170–300°C) due to the dihydroxylation of ceria gel. In conclusion, both ceria and stania are thermally stable after 300 and 400 °C., respectively.

Fig. 2 illustrates the XRD patterns of SnO₂ and CeO₂ calcined at 600 °C. This figure exposes the XRD pattern of SnO₂ with peak values of 26.5°, 33.8°, 39°, 51.7°, 54.2°, 62.0°, 64.8°, 66.0° and 68.1° which is assigned to [110], [101], [200], [211], [220], [310], [112], [301], and [202] planes, respectively. Thus the obtained XRD patterns toward the rutile (tetragonal) SnO₂ phase (ASTM card No. 41-1445) [35, 36]. While the XRD diffractogram of CeO₂ showed sharp and intense peaks at $2\theta = 28.6^\circ, 33.1^\circ, 47.6^\circ, 56.2^\circ$ and 59.1° which can be attributed to the [111], [200], [220], [311], and [222] respectively, corresponding to cubic ceria fluorite structure as matched with the database in JCPDS file number 04-0593 [36-39]. From the XRD pattern, the average crystallite sizes, calculated from Debye-Scherrer's equation, of SnO₂ and CeO₂ were found to be 18 and 44 nm, respectively (see **Table 1**).

Fig. 3 depicts the TEM images and average particle size distribution of ceria and stania. The TEM images reveal

a spherical topography of the prepared nanoparticles. The TEM analysis confirms the formation of nanoparticles with average sizes of 22.5 nm for stania and 45.4 nm for ceria, which aligns with the results obtained from XRD analysis. Additionally, the TEM analysis indicates that the synthesized nanoparticles exhibit a slightly irregular and rounded shape.

Nitrogen adsorption/desorption isotherms at -196 °C for both SnO₂ and CeO₂ catalysts are shown in **Fig. 4**, and the resulted data were cited in **Table 1**. The isotherms of both catalysts stania and ceria belong to Type IV and the hysteresis loop of Type H3 mixed with H2 according to IUPAC classifications which are characteristic for porous materials [36]. And for both isotherms, the closer point of the hysteresis loops lies at P/P₀ = 0.4 and 0.2 for SnO₂ and CeO₂, respectively. This means that the complete monolayer formation takes place slowly for stania compared to ceria and there is an effective impact of micropores to the adsorption on the SnO₂ catalyst more than CeO₂. Values of the surface area of the catalysts are estimated from BET curves and cited in **Table 1**. Both SnO₂ and CeO₂ have comparable surface area ($S_{BET} = 11 \text{ m}^2 \text{ g}^{-1}$ for SnO₂ and $12 \text{ m}^2 \text{ g}^{-1}$ for CeO₂), this is well agreed with the previous data [40].

Table 1 Surface area and crystallite size

Sample	pHzpc ^(a)	Band Gap ^(b) eV	S _{BET} m ² /g	Tota pore volume (cm ³ /g)	Crystallite Size (nm)
Ceria	8.1	3.23	12	0.0764	44
Stania	5	3.60	11	0.0325	18

(a) [41, 42] (b) [22, 23]

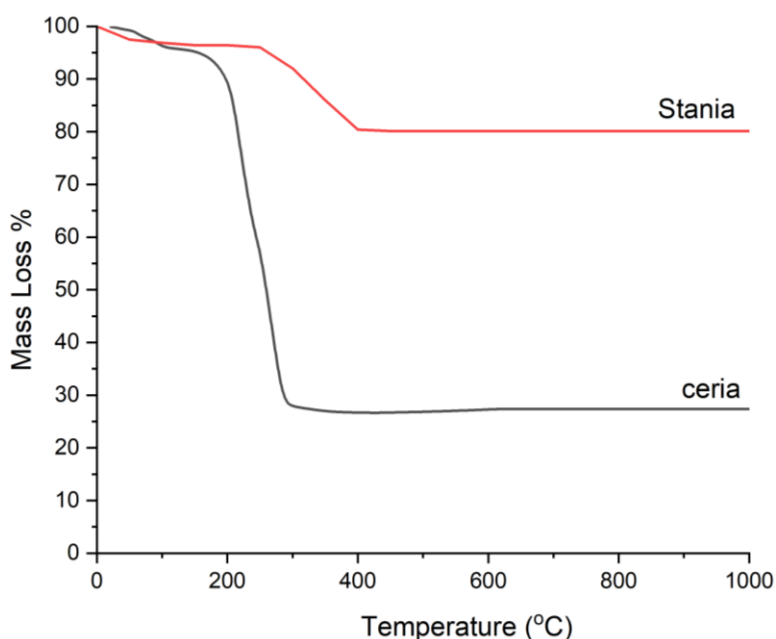


Fig. 1 TGA of ceria and stania catalysts (from RT- 1000 °C in a static air, 5-15 mg of the sample and 10°C /min rate of heating).

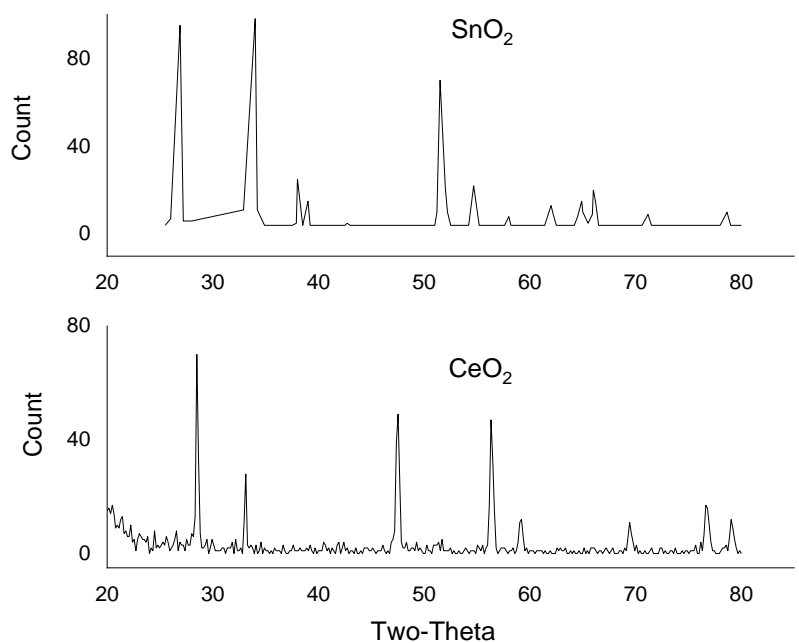


Fig. 2 XRD of ceria and stania catalysts (scanning rate of $2^\circ\theta / \text{min}$)

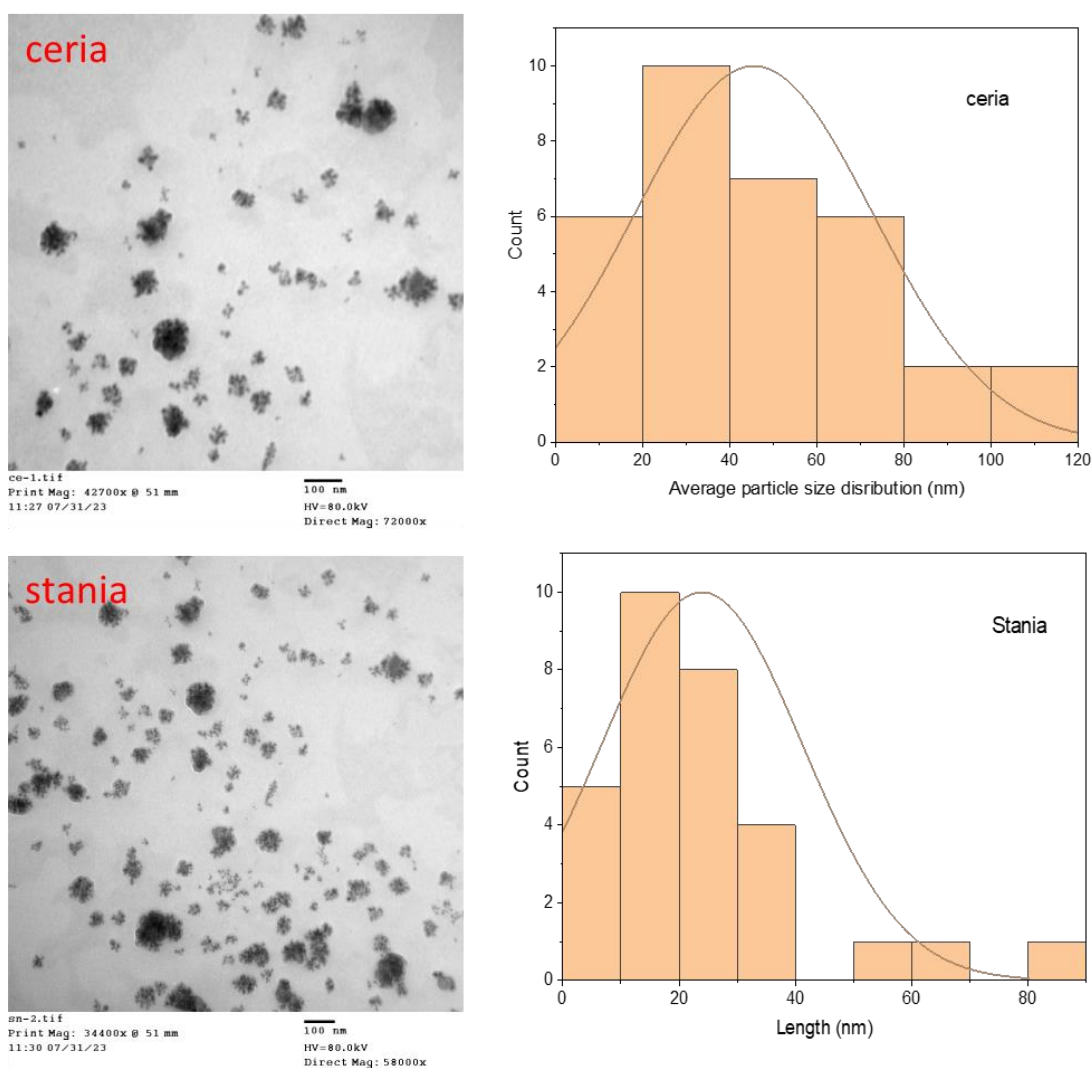


Fig. 3 TEM image and average particles size distribution obtained by applying image-j software on TEM images.

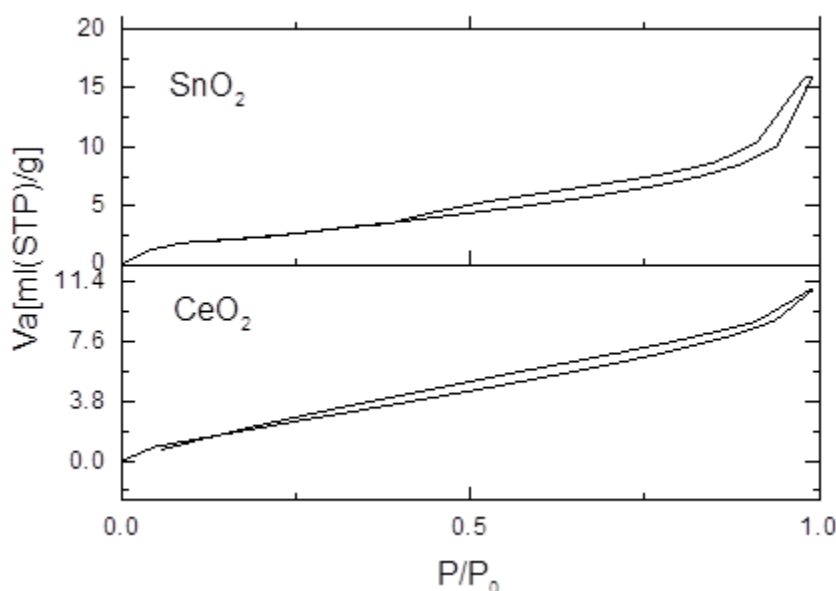


Fig. 4 N₂ sorption isotherms of ceria and stania catalysts (at -196 °C)

3.2 Effective UV Wavelength

To know which wavelength is the most effective on the degradation process, initial UV photolysis experiments were conducted at pH = 9 for 120 minutes with both UV lamps available (with wavelength 254 and 365 nm). Results are shown in **Table 2**. Experiments were run for 120 minutes to eliminate the effect of exposure time. Results in Table 2 show that the shorter wavelength (254 nm) was significantly more effective on the degradation of TEN in water than the longer wavelength (365 nm). The Deg. % of TEN at wavelength 254 and 365 nm is found to be 87.6 and 29.8 respectively. The full UV scan of TEN shows that it absorbs light below 300 nm. Hence, no significant degradation was expected due to 365 nm UV irradiation. This agrees with the data reported previously [43, 44], and therefore the short wavelength was used for all experiments with different systems; CeO₂/UV/H₂O₂ and SnO₂/UV/H₂O₂.

3.3 Effect of pH and irradiation time on the degradation of TEN

The pH is an important factor since it affects the surface charge properties of the oxides. To study the effect of pH on the degradation of TEN, experiments were conducted by varying the pH in the range 3–11. The experimental conditions are 20 mg/L for TEN concentration, 120 min for the time of irradiation, H₂O₂ 300 mg/L, and the mass of the catalyst is 0.2 g. By

considering the characteristics of the catalyst and antibiotic at various pH levels, it is possible to interpret the pH on the photo-degradation of TEN antibiotics. Tenoxicam is a weak acid with pKa values of 5.3 and 1.1 [45]. Since the cationic antibiotic TEN has a positive charge in solution, the electrostatic adsorption model, which assumes that cations are more readily accumulated at the negative sites on oxides CeO₂ and SnO₂, can be used to explain how pH affects the photocatalytic degradation of TEN. This can be explained on the basis of the pH at the potential of zero-point charge, pH_{zpc}, of catalyst particles. The pH_{zpc} of CeO₂ and SnO₂ powder was 8.1 and 5, respectively [41, 42]. Above these pH values, the surfaces of ceria and stania were negatively charged by the adsorbed OH⁻ ions on the catalyst surface, while below this pH value, they are positively charged by the adsorbed H⁺ ions on the surface [46]. The results revealed maximum efficiency at basic pH. At basic pH, the photocatalyst surface becomes negatively charged attracting TEN molecules, positively charged, and hence higher degradation rate. So, keeping the medium of degradation at pH 9, the optimum amounts of degradation percent was attained (**Figs. 5, 6** and **Table 3**). On the other hand, at lower pH the electrostatic repulsion between the TEN cations and positively charged ceria and stania surface greatly reduces the adsorption of the TEN results in decrease in degradation percent.

Table 2 Effect of UV Wavelength (C₀ of TEN is 50 mg/L)

Wavelength (nm)	Total time (min)	pH	%Degradation
254	120	9	87.6
365	120	9	29.8

Additionally, the reaction between hydroxide ions and photo-induced holes on the catalyst surface, which produces hydroxyl radicals, was influenced by the pH of the solution. Positive holes are assumed to be the primary oxidation processes at low pH levels, whereas hydroxyl radicals are thought to be the major species at neutral or high pH levels. [41]. Because there were more readily available hydroxyl ions on the catalyst surface,

it would be expected that the generation of $\bullet\text{OH}$ would be higher. As a result, high pH logically increased the process's efficiency of deterioration. The degradation percentage of TEN in the presence of stania is larger than that of ceria, according to the results from **Figs. 5, 6**, and **Table 3**, and the lengthening of the irradiation period increased the degradation power.

Table 3 Maximum degradation % for TEN over ceria and stania at different pH (TEN concentration is 20 mg/L, time of irradiation is 120 min, mass of oxide is 0.2 g, and H_2O_2 300 mg/L).

pH	3	5	7	9	11
Ceria (Deg.%)	12	14.6	48.5	76	84
Stania (Deg. %)	22	32	62	91	93

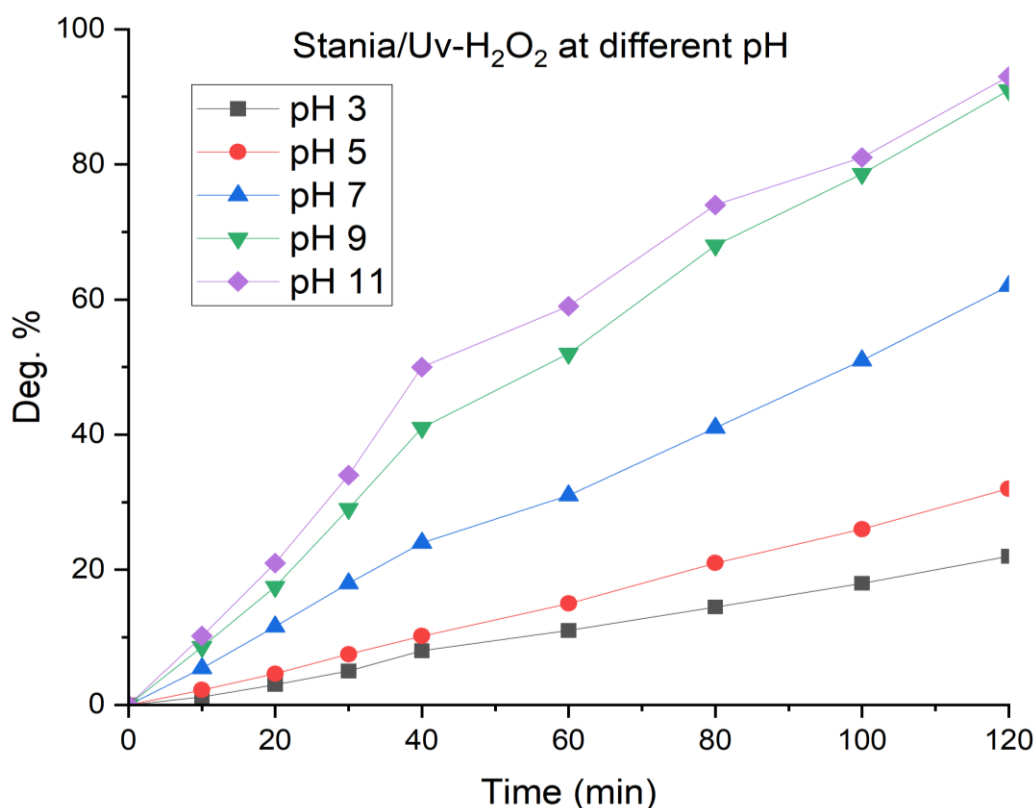


Fig. 5 photocatalytic degradation of TEN at different pH using stania/UV- H_2O_2 (TEN concentration is 20 mg/L, mass of stania is 0.2 g, and H_2O_2 300 mg/L).

3.4 Effect of catalyst mass on the degradation of TEN

To investigate the effect of catalyst loading on the degradation rate, several experiments were conducted at catalyst loading from 0.05 to 0.4 g/100 ml, pH 9, antibiotic concentration 20 mg/L, time of irradiation is 120 min, and H_2O_2 300 mg/L. **Fig. 7** clearly indicates that the increase in loading of the catalyst increases the rate of degradation up to a certain loading amount (0.3 g/100ml). The increase in degradation percent may be explained by the division of catalyst which produces

higher surface area. Subsequently with further increase in the loading level of the catalyst over 0.2 g/100 ml the degradation percentage starts diminishing (from 75 to 69% for ceria and from 87.5 to 80% for stania). This is due to the screening effect i.e., above a certain amount of loading, the turbidity of the solution increases resulting in the scattering of ultraviolet rays, hence reducing the optical path [47]. This decreases the percent of degradation above an optimum catalyst loading (0.2 g/100 mL).

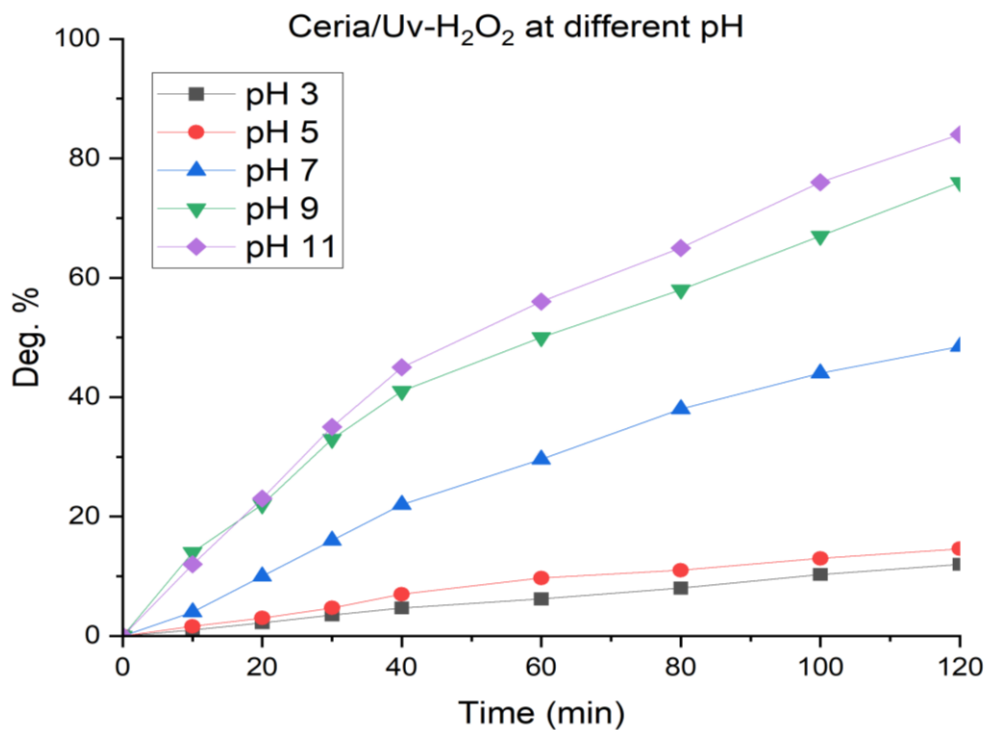


Fig. 6 photocatalytic degradation of TEN at different pH using ceria/UV-H₂O₂ (TEN concentration is 20 mg/L, mass of ceria is 0.2 g, and H₂O₂ 300 mg/L).

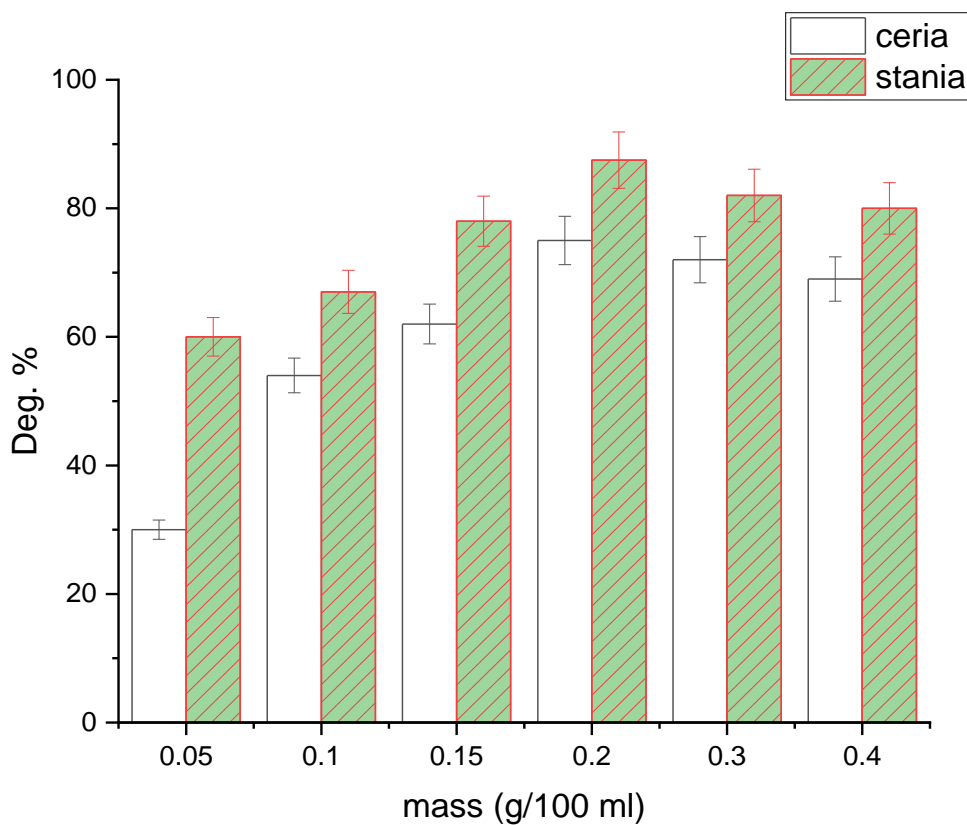
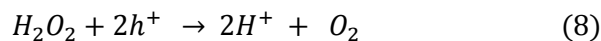
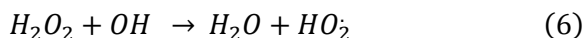


Fig. 7 photocatalytic degradation of TEN at different mass of catalysts (pH 9, TEN concentration 20 mg/L, time of irradiation is 120 min, and H₂O₂ 300 mg/L).

3.5 Effect of H₂O₂ on the degradation of TEN

The rate of photocatalytic degradation is greatly influenced by oxidant concentration. To conduct this effect, different concentrations of H₂O₂ were performed at constant pH (9), fixed concentration of TEN (20 mg/L), and mass of oxide is 0.2 g. The H₂O₂ concentration varied from 100-500 mg/L. **Fig. 8** clearly indicates the effect of H₂O₂ concentration on degradation efficiency of UV/catalyst/H₂O₂ process. For this process, with the increase in H₂O₂ concentration, the degradation percent increased till optimum H₂O₂ concentration is reached (300 mg/L). Further increase in H₂O₂ concentration lowered the degradation rate. This is due to the fact that excess H₂O₂ reacts with previously formed hydroxyl radicals and inhibits degradation by consuming the hydroxyl radicals that are responsible for breaking down the pollutant molecule, see equations 6-8, these results are in agreement with the previous reported [48-50]. Also, it is noticed that the degradation of TEN in case of stania is higher than that of ceria.



3.6 Antibiotics sorption

Sorption tests were performed in a reactor containing 100 ml of TEN solutions with an initial concentration of C₀ 20 mg/L, 300 mg/L H₂O₂, 0.2 g of the catalyst powder, ceria or stania, and the pH of solutions adjusted at 9. The amount of TEN adsorbed (q_t mg/g) was calculated from the difference between the initial concentration C₀ and the measured concentration (C_t) in the solution at time t, using equation (3). The kinetics of TEN sorption on both oxides were studied using the indicated conditions and illustrated in **Fig. 9**. From these figures, the maximum amount of TEN adsorbed (q_t) is about 7.2 and 8.7 mg. g⁻¹ for ceria, and stania, respectively. The adsorption kinetics of stania for TEN antibiotics was quick in the beginning, unlike ceria. For ceria, the adsorption equilibrium was established in about 60 min, but this time is decreased to 40 min in the case of stania. After this period, the degradation percentage did not change significantly with time.

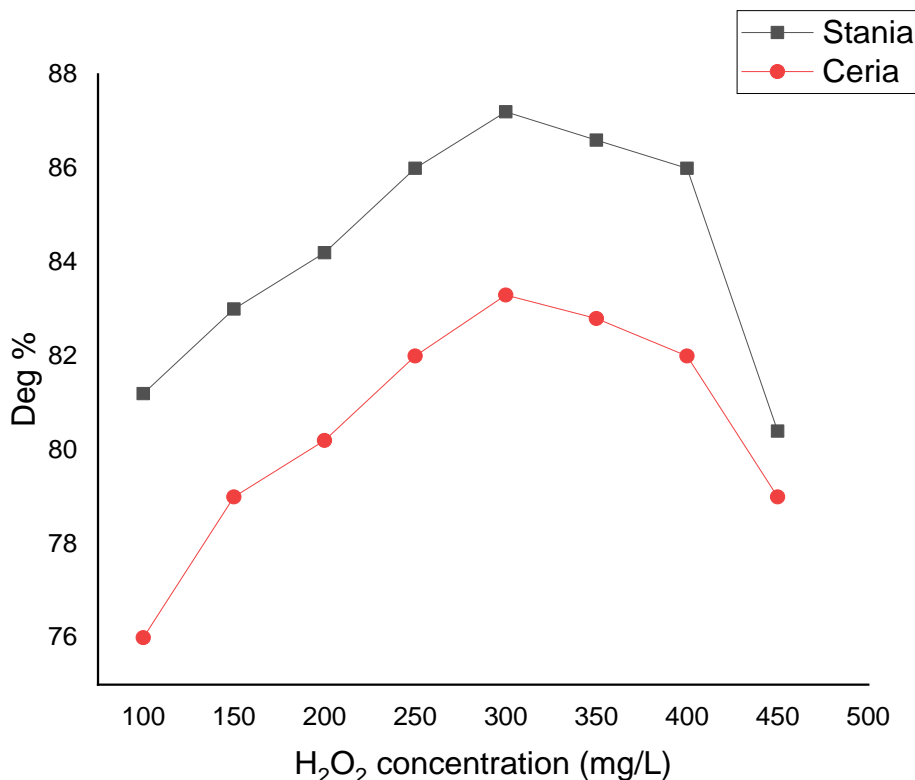


Fig. 8 photocatalytic degradation of TEN at different H₂O₂ concentration using ceria and stania (at pH 9, concentration of TEN (20 mg/L), and mass of catalyst is 0.2 g)

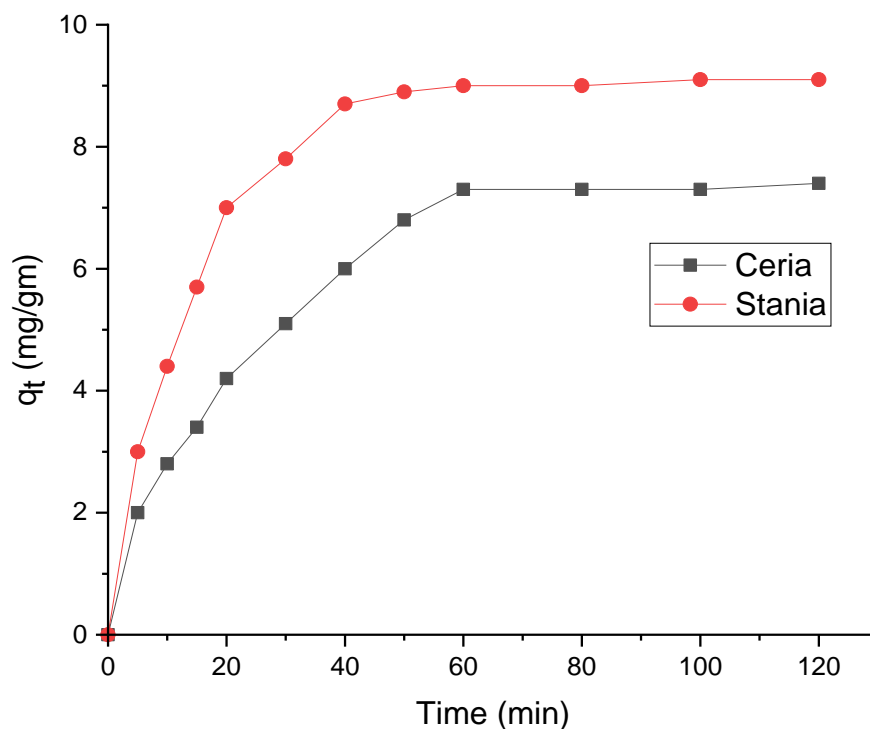


Fig. 9 kinetics of TEN sorption on ceria and stania ($C_0 = 20$ mg/L), 300 mg/L H_2O_2 , mass of catalyst 0.2 g and pH 9)

3.7 Kinetic of the photodegradation

The kinetics study of TEN photodegradation using ceria and stania was evaluated for UV/ H_2O_2 /oxide systems and were conducted under optimum operating conditions (C_0 20 mg/100 ml, 300 mg/L H_2O_2 , mass of catalyst 0.2 g/100 ml and pH 9). The degradation of TEN was observed as a function of irradiation time and data were fitted to a first-order rate model using equation (4). In comparison to the kinetic curves associated to the photocatalytic process (**Fig. 10**), stania is faster than ceria to degrade TEN antibiotics in water relating to its high sorption capacity in dark conditions. The plot of $\ln C_0/C_t$ versus time (**Fig. 11**) exhibits a straight line, the straight line of the plots suggests that the photocatalytic reaction followed the pseudo-first order kinetics and it became clear both oxides have an

advantage in removing TEN from aqueous solutions. The calculated rate constant and half- lifetime are given in **Table 4**. The results showed that the pseudo first-order kinetic model can describe the photocatalytic degradation of TEN antibiotics for both catalysts. It can be predicted that the significant difference in degradation rates might be due to the difference in surface properties between both ceria and stania catalysts. Moreover, the K_1 constant is larger with the stania catalyst ($K_1 \approx 1.86 \times 10^{-2} \text{ min}^{-1}$), compared to that of ceria ($K_1 1.54 \times 10^{-2} \text{ min}^{-1}$). The findings align well with stania's higher porosity compared to ceria. The results obtained validate that as the size of the crystallite increases, the rate constant decreases and the half-life time tends to increase. It is observed that the degradation process is more pronounced for smaller crystallite sizes [51, 52].

Table 4 kinetics data according to pseudo 1st order model

Sample	Rate constant ($K_1 \times 10^{-2}$) min^{-1}	Half lifetime $t_{1/2}$ (min)	R^2
Ceria	1.54	45	0.994
Stania	1.86	37	0.997

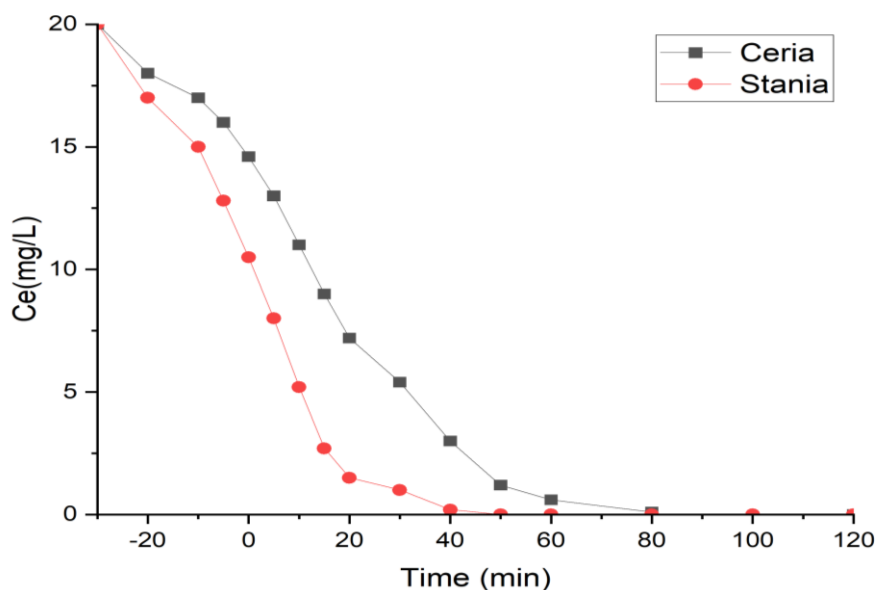


Fig. 10 Photodegradative efficiency of TEN over ceria and stania catalysts (C_0 20 mg/100 ml, 300 mg/L H_2O_2 , mass of catalyst 0.2 g/100 ml and pH 9).

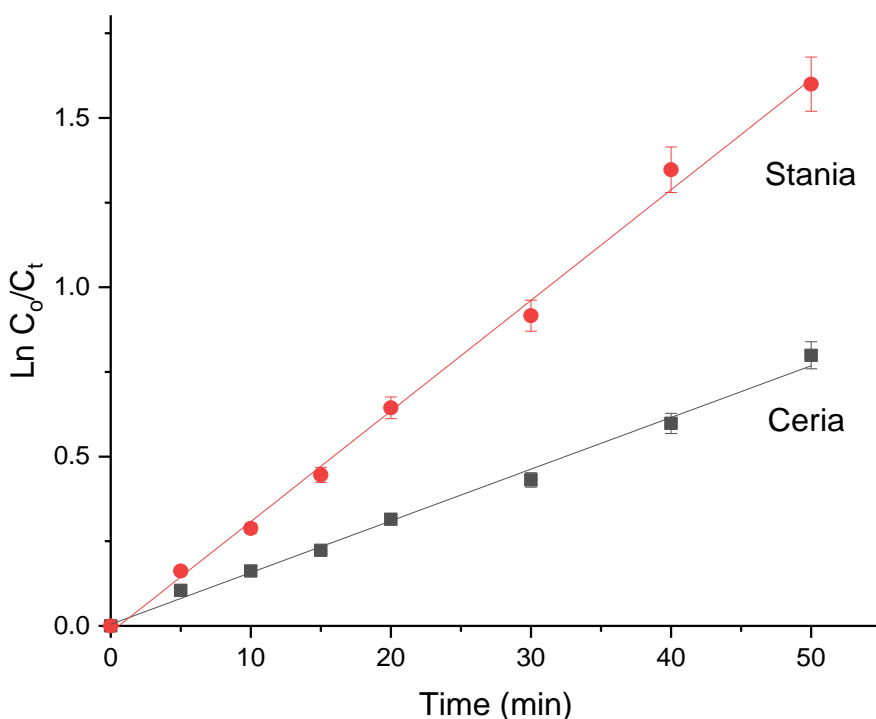


Fig. 11 Kinetic analysis of TEN degradation over ceria and stania (C_0 20 mg/100 ml, 300 mg/L H_2O_2 , mass of catalyst 0.2 g/100 ml and pH 9).

4. Conclusions

Ceria and stania catalysts were prepared using a precipitation method. Dried CeO_2 powder exhibits fluorite structure and the average crystallite size is found to be 44 nm higher than that of stania (18 nm). The S_{BET} of both oxides are comparable to 12 and 11 m^2/g for ceria and stania, respectively. Data obtained show that both oxides, ceria and stania can be used effectively as

catalysts in the photodegrading process as photocatalyst. Stania is faster than ceria to degrade TEN antibiotics. Ceria needs more time than stania to degrade the drug at 100%, in which the TEN is fully degraded in the presence of stania and H_2O_2 at 40 min under certain conditions.

Acknowledgements

The authors would like to thank Dr. Nadia O. El-Gamal, Asyut University, for her assistance in the BET, TGA, and TEM analysis.

References

- [1] V. Homem and L. Santos. *J. Environ. Manage.* 92 (2011) 2304-2347.
- [2] D. Klauson, J. Babkina, K. Stepanova, M. Krichevskaya, and S. Preis. *Catal. Today*, 151 (2010) 39-45.
- [3] V.J. Pereira, K.G. Linden, and H.S. Weinberg. *Water Res.*, 41 (2007) 4413-4423.
- [4] C. EL Bekkali, H. Bouyarmane, S. Laasri, A. Laghizil, and A. Saoiabi. *Iran. J. Catal.*, 8 (2018) 241-247.
- [5] M. Nosuhi and A. Nezamzadeh-Ejhih. *J. Colloid Interface Sci.*, 497 (2017) 66-72.
- [6] S. Kim, P. Eichhorn, J.N. Jensen, A.S. Weber, and D.S. Aga. *Environ. Sci. Technol.*, 39 (2005) 5816-5823.
- [7] T.A. Larsen, J. Lienert, A. Joss, and H. Siegrist. *J. Biotechnol.*, 113 (2004) 295-304.
- [8] N.H. Ince and G. Tezcanlı. *Dyes Pigm.* 49 (2001) 145-153.
- [9] V. Yargeau and C. Leclair. *Ozone: Sci. Eng.*, 30 (2008) 175-188.
- [10] O. González, C. Sans, and S. Esplugas. *J. Hazard. Mater.* 146 (2007) 459-464.
- [11] T.E. Doll and F.H. Frimmel. *Chemosphere*, 52 (2003) 1757-1769.
- [12] L. Rizzo, S. Meric, D. Kassinos, M. Guida, F. Russo, and V. Belgiorno. *Water Res.*, 43 (2009) 979-988.
- [13] W. Hu and X. Yuan. *J. Nanomat.*, 2017 (2017) 1-6.
- [14] S.K. Kansal, P. Kundu, S. Sood, R. Lamba, A. Umar, and S. Mehta. *New J. Chem.*, 38 (2014) 3220-3226.
- [15] Y.-H. Jin, K.-M. Min, S.-D. Seo, H.-W. Shim, and D.-W. Kim. *J. Phys. Chem. C*, 115 (2011) 22062-22067.
- [16] Y. Lei, F. Qu, and X. Wu. *Nano Micro Lett.* 4 (2012) 45-51.
- [17] L. Yu, F. Qu, and X. Wu. *Appl. Surf. Sci.*, 257 (2011) 7432-7435.
- [18] H. Liu, M. Wang, Y. Wang, Y. Liang, W. Cao, and Y. Su. *J. Photochem. Photobiol., A*, 223 (2011) 157-164.
- [19] B. Choudhury, P. Chetri, and A. Choudhury. *RSC Adv.*, (2013).
- [20] Y. Zhai, S. Zhang, and H. Pang. *Mater. Lett.*, 61 (2007) 1863-1866.
- [21] A. Kathiravan, M.A. Jhonsi, and R. Renganathan. *J. Lumin.*, 131 (2011) 1975-1981.
- [22] M. Karmaoui, A.B. Jorge, P.F. McMillan, A.E. Aliev, R.C. Pullar, J.o.A.n. Labrincha, and D.M. Tobaldi. *ACS Omega*, 3 (2018) 13227-13238.
- [23] C.N. Pham, Q.V. Trinh, T.V. Dang, N.N. Dao, B.Q. Nguyen, D.T. Doan, H.B. Le, V.V. Nguyen, L.T. Duong, and L.D. Tran. *Adsorpt. Sci. Technol.*, 2022 (2022) 1-12.
- [24] Y.-S. Li, A. Fang, G.-J. Lee, J.J. Wu, Y.-C. Chang, C.-Y. Tsay, J.-H. Chen, T.-L. Horng, and C.-Y. Chen. *Catalysts*, 10 (2020) 732.
- [25] H. Derikvandi and A. Nezamzadeh-Ejhih. *J. Hazard. Mater.* 321 (2017) 629-638.
- [26] A. Yousefi and A. Nezamzadeh-Ejhih. *Iran. J. Catal.*, 11 (2021) 247-259.
- [27] J.R. Patel, R.A. Carlton, F. Yuniatine, T.E. Needham, L. Wu, and F.G. Vogt. *J. Pharm. Sci.*, 101 (2012) 641-663.
- [28] S.S. Mahmoud, M.A. Hassan, F.H. El-Khatib, A.A. Obaidat, and M. Sheikh-Salem. *React. Kinet. Catal. Lett.* 70 (2000) 119-124.
- [29] M.M. de Melo Santos, T.D. Da Silva, A.L.A. De Lucena, D.C. Napoleão, and M.M.M. Duarte. *Water Air Soil Pollut.*, 231 (2020) 1-15.
- [30] M.M.d.M.S. Moura, V.E. Lima, A.A.d.M. Neto, A.L.A.d. Lucena, D.C. Napoleão, and M.M.M. Duarte. *Water Sci. Technol.*, 83 (2021) 863-876.
- [31] Q.-y. Liu, F. Yang, Z.-h. Liu, and G. Li. *J. Ind. Eng. Chem.*, 26 (2015) 46-54.
- [32] B.D. Cullity, *Elements of X-ray Diffraction*. 1956: Addison-Wesley Publishing.
- [33] V. Ramasamy, K. Praba, and G. Murugadoss. *Spectrochim. Acta, Part A.*, 96 (2012) 963-971.
- [34] N. Omrani and A. Nezamzadeh-Ejhih. *Sep. Purif. Technol.*, 235 (2020) 116228.
- [35] S. Nagarani, G. Sasikala, K. Satheesh, M. Yuvaraj, and R. Jayavel. *J. Mater. Sci.: Mater. Electron.*, 29 (2018) 11738-11748.
- [36] H.A. Khalaf, S.E. Mansour, and E.A. El-Madani. *J. Assoc. Ar. Univ. Basic Appl. Sci.*, 10 (2011) 15-20.

- [37] R. Radha, J. Johny, K. Madan, and G.R. Rao. *Mater. Lett.*, 323 (2022) 132587.
- [38] A. Chen, Z. Zhang, X. Li, and Y. Chen. *J. Mater. Sci.: Mater. Electron.*, 27 (2016) 2919-2925.
- [39] H. Pouretedal, Z. Tofangsazi, and M. Keshavarz. *J. Alloys Compd.*, 513 (2012) 359-364.
- [40] H.A. Khalaf. *SpringerPlus*, 2 (2013) 619.
- [41] J.J. Gulicovski, I. Bračko, and S.K. Milonjić. *Mater. Chem. Phys.*, 148 (2014) 868-873.
- [42] E. Youssof, M. Tammam, Y. Abdel-Mottaleb, and M.S. Abdel-Mottaleb. *Egypt. J. Chem.*, 64 (2021) 425-430.
- [43] I. Elghamry, M.C. Letzel, and J. Mattay. *Trends Photochem. Photobiol.*, 14 (2012) 21-25.
- [44] A. Voulgari, D. Benaki, S. Michaleas, and E. Antoniadou-Vyza. *J. Inclusion Phenom. Macrocyclic Chem.*, 57 (2007) 141-146.
- [45] A.M. Al-Obaid and M.S. Mian, Tenoxicam, in *Analytical profiles of drug substances and excipients*. 1993, Elsevier. p. 431-459.
- [46] B. Divband, A. Jodaiei, and M. Khatamian. *Iran. J. Catal.*, 9 (2019) 63-70.
- [47] M.T. Uddin, Y. Nicolas, C. Olivier, T. Toupance, L. Servant, M.M. Muller, H.-J. Kleebe, J. Ziegler, and W. Jaegermann. *Inorg. Chem.*, 51 (2012) 7764-7773.
- [48] M. Zanjanchi, A. Ebrahimian, and M. Arvand. *J. Hazard. Mater.*, 175 (2010) 992-1000.
- [49] A. Dixit, A. Mungray, and M. Chakraborty. *second International Conference on Chemical, Biological and Environmental Engineering*. 2010. IEEE.
- [50] S. Apollo, M.S. Onyongo, and A. Ochieng. *Iran. J. Chem. Chem. Eng.*, 33 (2014) 107-117.
- [51] B. Manikandan, K. Murali, and R. John. *Iran. J. Catal.*, 11 (2021) 1-11.
- [52] S. Salesi and A. Nezamzadeh-Ejhieh. *Environ. Sci. Pollut. Res.*, 29 (2022) 90191-90206.